# A Rolling Contact Joint Lower Extremity Exoskeleton Knee

Jonas Beil and Tamim Asfour

High Performance Humanoid Technologies Lab ($H^2T$), Institute for Anthropomatics and Robotics, Karlsruhe Institute of Technology (KIT), Germany
{jonas.beil, asfour}@kit.edu

**Abstract.** This paper presents the design, kinematics modeling and experimental evaluation of a rolling contact joint for usage as a knee joint in lower limb exoskeletons. The goal of the design is to increase wearability comfort by exploiting the migrating instantaneous joint center of rotation which is characteristic for rolling contact joints. Two 3D-printed parts with convex surfaces form the mechanism, which is coupled by two steel cables and driven by a linear actuator. This coupling allows rotations around all axis as well as predefined translations. We conducted a kinematic simulation to optimize the shape of the convex joint surfaces and to estimate the expected misalignment between the subject's knee and exoskeleton joint. In our experimental evaluation we compared forces measured at the exoskeleton interface between subject and exoskeleton prototype with attached rolling contact or revolute joint. The results indicate a reduction of forces and therefore increased kinematic compatibility of the proposed joint design.

**Keywords:** wearable robot, joint mechanism, exoskeleton knee joint

## 1 Introduction

Remarkable research efforts regarding the development of lower limbs exoskeletons have been made in recent years with the goal of improving the wearabilty and comfort of such devices. For exoskeletons designed for augmentation of human performance these are key requirements to increase user acceptance and allow the application of such exoskeletons in real world settings. Considering the human knee anatomy in the design process of a lower limb exoskeleton is therefore crucial to achieve high comfort and wearability as well as to prevent injuries caused by interaction forces at the interface during repetitive movements of the knee during walking. To this end, most commercial and many research lower limb exoskeletons use revolute joints to replicate the motion of the knee accepting macro and micro misalignments in order to keep the mechanical design as simple as possible ([1], [2], [3], [4]).

Other approaches align the instantaneous centers of rotation (ICR) of the human knee and the exoskeleton in the sagittal plane by utilizing additional joints. In [5], a cam mechanism for this alignment has been realized to follow the anatomical path of the knee joint axis during flexion motion while other systems use the four bar linkage mechanism [6], a Schmidt coupling [7] or a series of three revolute joints with parallel joint axis [8].

Since the knee is principally capable to perform rotations around all anatomical joint axis as well as translations in all spatial directions and the exoskeleton is coupled to the knee (parallel kinematics), exoskeletons with six degrees of freedom (DoF) were developed. The IT-knee uses a series of two articulated parallelograms, providing six degrees of freedom (DOF) to on the one hand self-align to the anatomy of different users and their knee articulation during motion and on the other hand to provide pure assistive torque to the flexion/extension axis [9]. In [10], a kinematic chain consisting of five revolute and one sliding joint is proposed to design an exoskeleton knee that self adjusts to the physiological knee movement. Both devices provide very good functionality but also require expanded space along the user's thigh and shank, impeding the implementation of hip or ankle joints.

**Fig. 1.** Prototype of the optimized rolling contact exoskeleton knee joint

In this paper, we present the conceptual design of a rolling contact joint (RCJ) for an knee exoskeleton for augmentation, which is capable of providing rotations around the anatomical joint axis as well as a prescribed translations of the ICR in the sagittal plane (see Fig. 1). The paper is organized as follows. In Section 2 the requirements for the system are derived from simulation of the human knee computing the translations projected to the assumed plane of the exoskeleton. The kinematic design and actuation of the device based on the requirements is described in Section 3. To gather indications of the kinematic compatibility a prototype was manufactured and used for experimental evaluation which is presented in Section 4. Section 5 concludes the paper.

## 2 Requirements

The knee joint as a condyloid hinge joint allows rotations around all anatomical axes and translations in all directions. However those rotations and translations are limited by the musculoskeletal system and are coupled to flexion/extension (F/E) motion during passive knee movement as previous studies have shown (see [11] and [12]). The instantaneous center of rotation (ICR) of the knee axis migrates on an evolute while the knee is flexed, rolling and sliding simultaneously [13]. Since the exoskeleton is placed parallel to the human knee and is coupled to the thigh and shank this could affect the required translations and rotations it has to perform.

Therefore, a kinematic simulation was set up which allows the projection of knee articulations to a parallel exoskeleton plane where the behavior of devices with different kinematic configurations could be investigated. Fig. 2 presents the basic structure of this simulation. To gather the required rotations and translations in the exoskeleton plane ($EP$), the knee joint is modeled as a four-link kinematic chain of cylindrical joints as described in [14], using the relations of Walker [11] to determine the translations ($S_1, S_2, S_3$).

Knee joint rotations ($\theta_1, \theta_2, \theta_3$) of a walking movement where gathered from [15], where the joint angles of five healthy subjects (mean age: 27 years, mean height: 180.6 cm, mean body mass: 75.2 kg) were measured with markers fixed to the tibia and femur with intra-cortical traction pins. The walking movement was chosen because it is assumed to be the most repeated motion while wearing the exoskeleton.

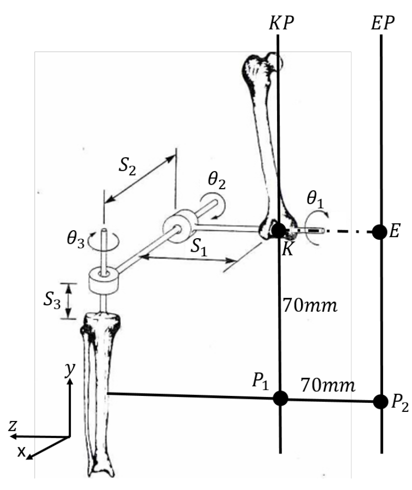


**Fig. 2.** Knee joint model labeled with the exoskeleton plane (EP), the knee plane (KP), the exoskeletons ICR (E) and the reference points on the user's leg (P1) and the exoskeleton (P2) used to determine the required trajectory of the exoskeleton joint (Figure adopted from [14])

The knee rotations and translations were projected from point $P_1$ in the sagittal plane ($KP$) to point $P_2$ in the exoskeleton plane ($EP$). Plane $EP$ is parallel to $KP$, has a distance of 70 mm in lateral direction to plane $KP$ and $P_1$ is placed 70 mm distal to the knee joint. $P_1$ is the location of the physical human robot interface (pHRI) connecting the human leg with the exoskeleton. The results of the simulation are presented in Fig. 3 showing the scatter-plot of the migrating point $P_1$ and its projection at $P_2$. The maximum translations in the XY-plane during a forward walking motion is 62.32 mm in x-direction and 39.33 mm in y-direction at a flexion angle of 65°.

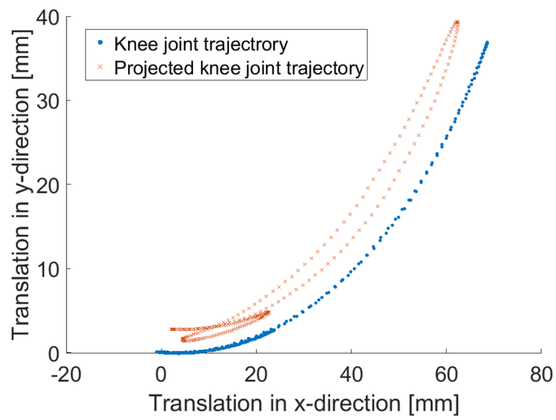


**Fig. 3.** Comparison of the knee joint trajectory at $P_1$ and its projection at $P_2$

The simultaneous appearance of flexion, abduction/adduction (ABD/ADD) and internal/external rotation (IR/ER) causes additional translations in the projection plane while the elliptic shape remains similar to the one observed in $KP$. Since the translations of $P_2$ will be used for further calculations, they will be denoted by $P_{refx,y,z}$.

The initial simulation is performed with a single revolute joint at point $E$ to compute a comparative value for later simulations with the proposed RCJ. Since this joint allows only rotations around $\theta_1$, misalignments and therefore unsolvable kinematic configurations occur during the simulation which are compensated with a 6DoF joint (three rotational and three translational DoFs) at point $K$. The 6 DoF joint should only deflect in the case of misalignment, so a spring stiffness of 9 N/m or 9 N/rad as well as a damping coefficient of 0.02 N/ms or 0.02 Nm/rads was added to all DoFs of the joint. All other joints have no stiffness or damping and are therefore preferred when solving the inverse kinematics. While running the simulation the deflections of the 6 DoF joint and the spatial position of $P_2$ are recorded 280 times per one gait cycle and the translations of $P_2$ are compared to $P_{refx,y,z}$ (see Equation 1).

$$F = \sum_{n} \left(6D_{x,y,z} + |P_{refx,y,z} - P_{2x,y,z}|\right) \; [m] \tag{1}$$

The variable $n$ denotes the number of recorded values and $6D_{x,y,z}$ are the translations of the 6 DoF joint. They are added to the absolute difference of the translations of the projected reference point $P_{refx,y,z}$ and the translations resulting from the motions of the revolute joint $P_{2x,y,z}$. The value of $F$ amounts to 49.009 m for the revolute joint while the ideal exoskeleton joint with six DoF would have an value of 0. Rotations of the 6 DoF joint are not taken into account in the equation because they correlate with the translations, meaning that a reduction of the observed translations at point $P_2$ and in the 6 DoF joint automatically leads to a reduction of the rotations.

The proposed exoskeleton knee joint should have a reduced value for $F$ and be capable of producing a similar shaped trajectory as presented in Fig. 3. Additionally, the range of motion (RoM) for the F/E axis is required to be equivalent to the human knee (i. e. 135°), while RoMs of the ABD/ADD and IR/ER axis should exceed the respective values arising in forward walking motions (ABD/ADD: 7.5°, IR/ER: 10°). The joint actuation is as important as the kinematic joint structure. Since the goal for our joint is to augment healthy people during working, the actuation should reduce peak torques around the F/E axis and if possible also around the ABD/ADD axis.

## 3 Design

As stated in Section 2, rolling and sliding motion influenced by the shape of femur and tibia in the human knee result in a migration of the ICR during flexion. Hence reproducing this behaviour would lead to a reduction on misalignments significantly. To achieve this we investigate the design of a system with two spheres forming a rolling contact joint. Similar system have already been proposed for robotic fingers ([16], [17]), prosthesis and other technical applications ([18], [19], [20]).

### 3.1 Modelling of the Rolling Contact Joint

The kinematics of bodies rolling on each other are well described in the literature e.g. in [21]. Fig. 4 presents the case where one cylinder is rolling on a non-moving second cylinder. The ICR migrates on a circle with a radius equivalent to the radius of the non-moving body while the resulting rotation $\alpha$ (corresponding to F/E) is the sum of $\alpha_1$ and $\alpha_2$. By providing two different radii for the bodies, the joint angle in relation to the joint translations can be changed (see Equation 2). Additionally, the moving cylinder can rotate around an axis along $r_2$ (corresponding to IR/ER) without moving the ICR in Fig. 4.

$$\alpha = \alpha_1 + \alpha_2 = \alpha_1 + \frac{r_1 \cdot \alpha_1}{r_2} \tag{2}$$

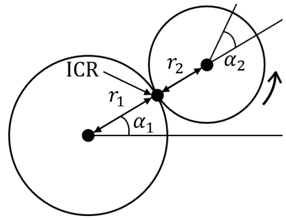


**Fig. 4.** Schematic drawing of a deflected RCJ in 2D

Replacing the two cylinders with two spherical bodies adds a third rotational DoF (corresponding to ABD/ADD) perpendicular to the aforementioned joint axis. This leads to the kinematic equivalent system shown in Fig. 5, which we used in our simulation. It consists of two revolute joints for the pitch (corresponding to F/E) and yaw (corresponding to ABD/ADD) axis each, as well as one revolute joint for the roll axis (corresponding to IR/ER) which are connected by links with a length equivalent to the radii $r_1$ and $r_2$. The rotation sequence is $Pitch_1$, $Yaw_1$, $Roll$, $Yaw_2$, $Pitch_2$. Using the simulation described in Section

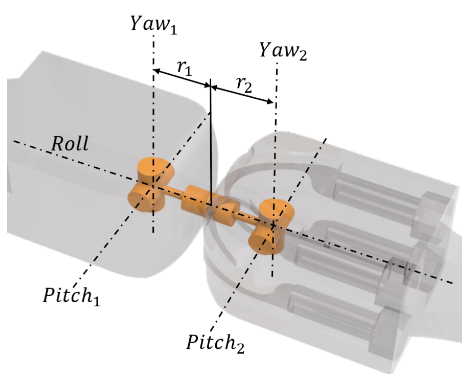


**Fig. 5.** Kinematic chain used to model the rolling contact joint (RCJ)

2 with the RCJ model, the behavior during the gait cycle can be investigated. Up to this point the values for $r_1$ and $r_2$are not defined. Since manual identification of the values is difficult and time consuming, an optimization process using the pattern search algorithm was included in the simulation. The algorithm minimizes the variable $F$ introduced in Section 2.

$$F_{opt} = min(F) \tag{3}$$

This means, that the translations of the 6 DoF joint ($6D_{x,y,z}$) have to be

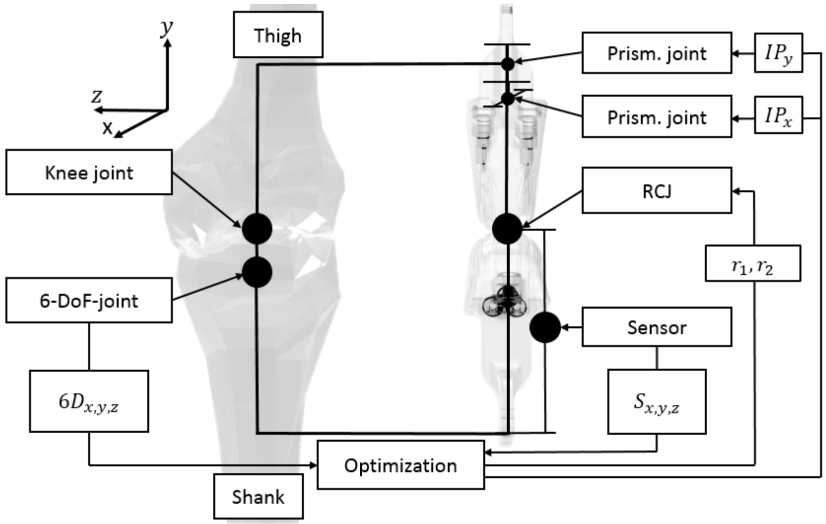


**Fig. 6.** Schematic of the simulation and optimization process

minimized and that the RCJ should follow the reference trajectory ($P_{refx,y,z}$) in the $EP$-plane as close as possible. Fig. 6 shows the schematic setup of the simulation as well as the variables which are used in the optimization process. In addition to $r_1$ and $r_2$ the initial position of the RCJ in the XY-plane described by $IP_x$ and $IP_y$ is varied by the pattern search algorithm. The last two parameters were introduced because the knee joint is abducted at the beginning of the gait cycle causing initial translations at the exoskeleton knee joint due to parallel kinematics. Table 1 summarizes the initial values, the lower and upper bounds as well as the final values of the optimization process.

The optimization function $F_{opt}$ sums to 2.422 m using the final values meaning a reduction of 7.37 m compared with the initial values. Fig. 7 presents the translations at the 6 DoF joint during one gait cycle, equivalent to the misalignment of the ICRs of exoskeleton and knee. Since no translations in z-direction were provided for the knee joint those values remain low (maximum translation of $-0.95$ mm in the swing phase). Translations in $x$ and $y$ direction show higher

**Table 1.** Optimized parameters of the RCJ

| **Parameter** | **Initial value [mm]** | **Lower/Upper boundary [mm]** | **Final Value [mm]** |
|---|---|---|---|
| $r_1$ | 20 | 10/30 | 11.4 |
| $r_2$ | 20 | 10/30 | 13.1 |
| $IP_x$ | 0 | $-50/50$ | 1.7 |
| $IP_y$ | 0 | $-50/50$ | $-4.2$ |

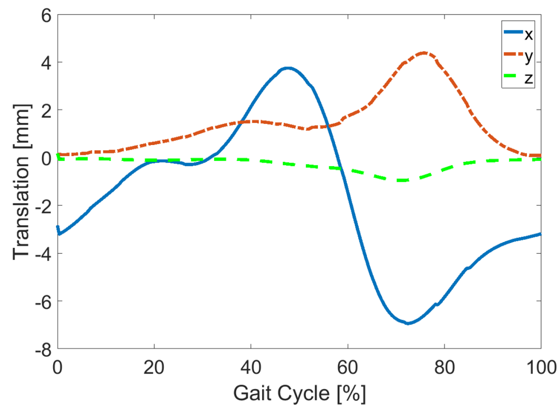


**Fig. 7.** Translations at the 6 DoF joint during one gait cycle

values especially during swing phase when the highest flexion occurs, since knee ICR migration is coupled to the flexion angle. Joint rotations of the 6 DOF joint are close zero ($\sim 10^{-5}\,rad$) during the whole simulation. Since the initial position of the revolute joint was not optimized, the parameters $IP_x$ and $IP_y$ were set so zero leading to a value of 3.009 m. Comparison to the revolute joint value derived in Section 2, results in a reduction of 46.081 m.

### 3.2 Mechanical Design

Two base components forming the RCJ (thigh and shank part) were designed using the final radii and width of the optimization process. They are connected by two steel cables with a diameter of 1.2 mm which are guided diagonally through the RCJ. Fig. 8 presents the construction which is also equipped with four adjustment screws to change the initial cable length and three profiled cam rollers.

Cable 1 starts at the adjustment screw of the anterior thigh side and is guided through the grooved contact surfaces to the posterior shank side. After passing the shank part it rotates around the profiled cam roller and is lead back to the thigh. Basically the same guiding is also used for cable 2 with the difference that the starting and end point is at the posterior thigh side. Assuming that both cables are equally pretensioned, this arrangement leads to torque equilibrium around all joint axis if the joint is undeflected. Since both convex part surfaces should stay in contact, the grooves have a depth of 1.5 mm to incorporate the 1.2 mm steel cables.

The rolling contact joint design prevents cable elongation (as well as arising joint torques) when the joint is deflected around the F/E axis. Joint deflections around the yaw or roll axis would lead to cable elongation. Therefore, the cables are guided over profiled cam rollers to compensate this elongation and only small torques occur caused by friction in the cable channels.

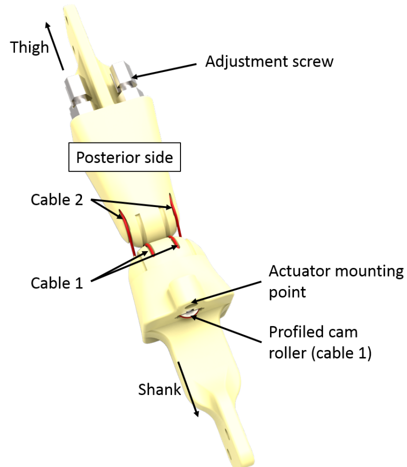


**Fig. 8.** Mechanical design of the RCJ

### 3.3 Actuation

As stated in Section 2 the actuation should reduce peak torques around the F/E axis and if possible also around the ABD/ADD axis. Therefore, a linear actuator mounted at the thigh part of the exoskeleton and the anterior actuator mounting point at the shank part (see Fig. 8) via ball bearings is proposed. Fig. 9 presents the actuation principle for a configuration with no joint deflection (left) and a configuration with deflected yaw and roll joint (right). These two cases will be investigated to compute the torques for F/E (first case) and analyze parasitic torques for IR/ER and ABD/ADD (second case). The second case was selected because the knee is mainly abducted during the gait cycle (max angle of 7.5°) combined with both internal and external rotation.

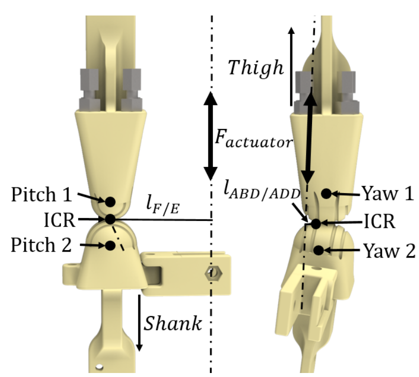


**Fig. 9.** Influence of joint deflections on the actuation

The lever arm to the pitch axis ($l_p$) amounts to 52.26 mm for an angle of 0° and reduces to 36.71 mm for a pitch angle of 90°. Using eq. 1, the motion of the ICR and the actuator mounting point during Abd. and IR/ER motions is calculated. Assuming an actuator length of 263 mm the direction of the actuator force is obtained. The resulting torque arm of $F_{actuator}$ to the yaw axis ($l_y$) amounts to 0.25 mm (0.6% of $l_p$) for an Abd. and IR. angle of 7.5°. For a combined motion around the Abd. and ER axis a lever arm $l_y$ of 1.29 mm (3.5% of $l_p$) is obtained.

The linear actuator introduced in our previous work (see [22]) has a maximum force of 900 N at 100 mm/s and was chosen to calculate the arising torques. With the aforementioned values a maximum torque of 47 Nm at 180 deg/s around the pitch axis is obtained. This parasitic torques around the yaw axis amount to 0.25 Nm for ABD. and IR. or 1.16 Nm for ABD. and ER. Since these values are low compared to the maximum torque in the pitch axis this result is considered acceptable.

## 4 Evaluation and Results

Two experiments were conducted to validate the simulation results. In the first experiment maximum joint angles of the prototype from Fig. 1 were measured. Therefore, the joint was manually deflected around all axis until a significant increase of joint stiffness was detected by the person that articulated the joint. In pitch direction the stiffness is consistently low until the rolling parts collide. Deflection around the yaw axis is initially possible at low stiffness, too. Increasing deflection causes collision of the cables with the edges of the grooves, guiding them. The same holds for a deflection around the roll axis. After collision, further joint deflection can only be obtained by elongating the cables, meaning a drastically increased joint stiffness. The values presented in Table 2 exceed the maximum joint angles occurring in our reference walking motion and the maximum angle in pitch direction is higher than the maximum active flexion of the human knee. Therefore, a prototype exoskeleton was manufactured to conduct further experiments.

**Table 2.** RoMs of the RCJ compared to the required joint angles

| | Yaw | Pitch | Roll |
|---|---|---|---|
| RCJ | 19.5° | 138° | 34° |
| Required | 7.5° | 135° | 10° |

### 4.1 Prototype

Our prototype, shown in Fig. 10 consists of two base components which hold the thigh and shank part of the RCJ and connect them to the user's leg via Velcro straps. To be able to adapt the RCJ as well as the revolute joint (17 B47=20, Otto Bock HealthCare GmbH, Duderstadt) to the subject's knee axes, four linear and two revolute joints are incorporated as well. These joints are adjusted during the donning process and are fixed during operation. It is possible to exchange the RCJ with the revolute joint while the user is wearing the device in order to provide equal conditions for the experiments (e.g. that the Velcro straps remain tightened while joints are exchanged).

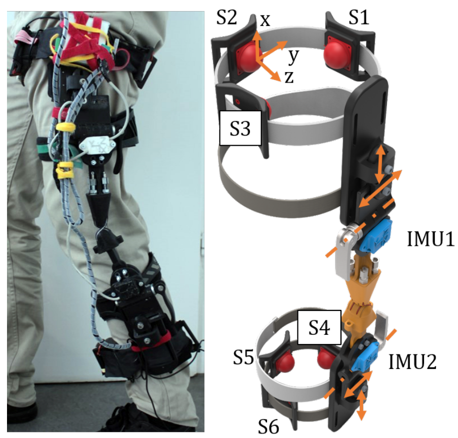


**Fig. 10.** Subject wearing the passive exoskeleton used during the experiments (left) and rendering presenting the sensor setup of the device (right)

The goal of the second experiment is to compare the kinematic compatibility of the RCJ to that of a revolute joint. Therefore, pressure and shear forces were measured with six 3D force sensors (Optoforce OMD-30-SE-100N, OptoForce Kft., Budapest) between the exoskeleton and the subject's leg, while the subjects is perfoming different motions wearing a passive exoskeleton. The sensors are mounted to 3D-printed interfaces and are positioned at posterior, medial and anterior side of the thigh and shank respectively. Due to the semi-spherical shape of the force sensors the maximum force, the resolution and the maximum dome deflection in compression direction (100 N, 6.25 mN, 3 mm) deviates from the aforementioned properties in shear direction (25 N, 7 mN, 2.5 mm). Two inertial measurement units (BNO055, Robert Bosch GmbH, Stuttgart) are utilized to compare joint deflections in the experiments.

### 4.2 Experiments

The experiments were conducted with three subjects with similar body characteristics (see Table 3) and the subject's knee axes was determined before donning the device. Then the exoskeleton with built-in RCJ was fixed to the user's leg by tightening two Velcro straps and the joint axis of RCJ and knee were adjusted using the aforementioned passive joints. Finally, the two Velcro straps with attached force sensors were tightened in a way that the forces were in between predefined intervals.

**Table 3.** Overview over basic body parameters of the three subjects

| Subjects | 3 male |
|---|---|
| Age | $27.33 \pm 5.03$ |
| Weight $[kg]$ | $72.00 \pm 3.46$ |
| Height $[cm]$ | $177.66 \pm 5.50$ |
| BMI $[kg/m^2]$ | $22.81 \pm 0.79$ |

Each subject had to perform a predefined set of movements starting with standing relaxed in an upright position. The forces measured while standing relaxed are used to calculate an offset to the forces of all other movements later. Subsequently seven other movements were performed: Walking four steps forward (1), crouching (2), turn left (3), turn right (4), four sidesteps (5), sit down on a chair and stand up (6). Every movement was recorded four times including the relaxed standing. The same procedure was repeated after mounting the revolute joint. Fig. 11 presents a comparison of the compression forces at the anterior thigh and the joint angles of the RCJ captured while executing one forward step. Negative values for $S6_z$ indicate compression forces since the sensor's z-axis is pointing away from it. In this trial, peak compression forces using the RCJ ($S6_zRCJ$) decreased by approximately 4 N while the progression of the force remains similar compared to forces when using the revolute joint. The highest forces occur during late stance ($40-60$ % of gait cycle) when the knee is extended. Reduced flexion angles (compared to literature) were observed for all

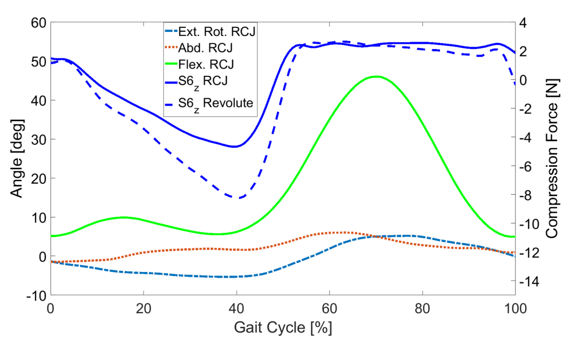


**Fig. 11.** Joint deflection and compression forces at the anterior thigh during one gait cycle

subjects conducting the experiments which can be explained by the compression of the thigh muscles caused by the Velcro strap. Abduction and rotation of the RCJ is similar to the observed angles in the human knee.

To gather indications about the kinematic compatibility, median and maximum values of all forces were calculated. First the median of the forces gathered from the standing motion was subtracted from all other joint values recorded with the same joint. Then all four trials of every movement were combined to one dataset to calculate its median and peak value. Table 4 summarizes the peak and median forces between the RCJ and the revolute joint of all sensors for the walking forward movement. This movement was selected because it was used exemplary during the whole design process. The third and six row denote the difference between the peak and median values of the two joints. Negative values indicate higher peak forces when using the revolute joint and vice versa. 24 out of 36 values show decreased peak forces ($S1_z \dots S6_z$) during the trials, while the most significant reductions occur on the medial sensors likely emerging from the enhanced mobility of the RCJ around the roll axis. Values of the posterior thigh sensor are mainly increased by the RCJ, which can be explained by an increased stiffness of the RCJ compared to the revolute joint, affecting the forces during stance phase (closed kinematic chain). Peak pressure forces are generally reduced ($S_2 \dots S_5$) or close to the value measured with the revolute joint ($S_1$). A similar force distribution was observed for the other movements as well. Combining all movements and peak forces leads to an average peak force reduction of 1.08 N.

To this end, the joint design has limitations regarding the joint angle sensing and the material wear. Since there are no distinct joint axis, joint angles were measured using IMUs which have a lower accuracy and tend to drift compared to other joint encoders. After the experiments significant wear of the 3D-printed surfaces rolling on each other was observed. It is not clear if this is caused by the assumed rolling motions or if there are slipping motions as well.

**Table 4.** Comparison of peak and median force values in all spatial directions between RCJ and revolute joint (all values in $[N]$)

| | Thigh | | | | | | | | | Shank | | | | | | | | |
|---|---|---|---|---|---|---|---|---|---|---|---|---|---|---|---|---|---|---|
| | $S_1$ | | | $S_2$ | | | $S_3$ | | | $S_4$ | | | $S_5$ | | | $S_6$ | | |
| | x | y | z | x | y | z | x | y | z | x | y | z | x | y | z | x | y | z |
| Peak RCJ | -3.3 | -1.6 | -4.0 | -1.2 | -1.1 | -1.5 | -1.5 | -1.3 | -1.8 | -0.8 | -1.6 | -1.7 | -1.5 | -1.5 | -3.4 | -0.6 | -0.9 | -3.7 |
| Peak Rev. | -2.6 | -1.1 | -3.7 | -2.4 | -2.7 | -2.3 | -4 | -2.1 | -3.3 | -0.7 | -1.9 | -2 | -3.1 | -1.4 | -4.8 | -0.5 | -1.3 | -4.6 |
| Diff. Peaks | -0.7 | -0.5 | -0.3 | 1.2 | 1.6 | 0.8 | 2.5 | 0.8 | 1.5 | -0.1 | 0.3 | 0.3 | 1.6 | -0.1 | 1.4 | -0.1 | 0.4 | 0.9 |
| Med. RCJ | -1.3 | -0.8 | -1.1 | -0.6 | -0.6 | -0.6 | -0.5 | -0.4 | -0.4 | -0.3 | -0.6 | -0.6 | -0.4 | -0.7 | -0.9 | -0.3 | -0.5 | -1.6 |
| Med. Rev. | -1.0 | -0.5 | -0.9 | -1.7 | -1.7 | -1.3 | -3.0 | -1.2 | -2.0 | -0.3 | -0.7 | -0.8 | -0.7 | -0.6 | -1.2 | -0.2 | -0.5 | -2.2 |
| Diff. Med. | -0.3 | -0.3 | -0.2 | 1.1 | 1.1 | 0.9 | 2.5 | 0.8 | 1.6 | 0.0 | 0.1 | 0.2 | 0.3 | -0.1 | 0.3 | -0.1 | 0.0 | 0.6 |

## 5 Conclusion and Future Work

We presented the conceptual design of a rolling contact joint intended to use as an exoskeleton knee mechanism, which is capable of performing three rotations and predefined translations in the sagittal plane to reduce macro- and micro-misalignments. Knee joint trajectories from literature served as simulation input to calculate the required rotations and translations in the plane where the device is assumed to be placed.

Our design consists of two parts with optimized shapes that are rolling on each other. The optimization was performed using a kinematic equivalent joint model coupled to a model of the human knee. The simulation results indicate increased alignment compared to a single revolute joint. The mechanical construction includes two cables to couple the rolling parts, which are guided over profiled cam rollers allowing joint deflection without cable elongation in a certain range around the Abd/Add. and IR/ER axes.

The resulting ranges of motions exceed knee angles while walking forward and the device provides a maximum flexion angle of 138°. Experimental evaluation to support the simulation results were also conducted. Indications regarding the kinematic compatibility were derived from the compression and shear forces captured with six 3D force sensors during multiple movements between the subject's leg and a prototype exoskeleton. To this end, forces with attached RCJ are compared to forces with attached revolute joint. The results indicate decreased compression and shear forces in five of the six sensors and therefore increased kinematic compatibility of the proposed joint design. Based on these promising results, we will conduct experiments using an actuated prototype to determine the forces between subject and exoskeleton for that case. The aforementioned limitations regarding joint angle sensing and wearability will be further addressed as well.

## Acknowledgment

This work has been supported by the German Federal Ministry of Education and Research (BMBF) under the project INOPRO (16SV7665).

## References

1. CYBERDYNE Inc. HAL Website (2018). [Online]. Available: www.cyberdyne.jp
2. EKSO Bionics website (2018). [Online]. Available: www.eksobionics.com
3. S. Wang and H. van der Kooij, "Modeling, Design, and Optimization of Mindwalker Series Elastic Joint," in *IEEE International Conference on Rehabilitation Robotics (ICORR)*, 2013, pp. 1–8.
4. S.-H. Hyon *et al.*, "Design of hybrid drive exoskeleton robot XoR2," in *IEEE/RSJ International Conference on Intelligent Robots and Systems (IROS)*, 2013, pp. 4642–4648.

5. D. Wang *et al.*, "Adaptive Knee Joint Exoskeleton Based on Biological Geometries," *IEEE/ASME Transactions on Mechatronics*, vol. 19, no. 4, pp. 1268–1278, 2014.
6. Kim *et al.*, "Development of the exoskeleton knee rehabilitation robot using the linear actuator," *International Journal of Precision Engineering and Manufacturing*, vol. 13, no. 10, pp. 1889–1895, 2012.
7. B. Celebi, M. Yalcin, and V. Patoglu, "AssistOn-Knee: A self-aligning knee exoskeleton," in *IEEE/RSJ International Conference on Intelligent Robots and Systems (IROS)*, 2013, pp. 996–1002.
8. B. Choi *et al.*, "A self-aligning knee joint for walking assistance devices," in *International Conference of the Engineering in Medicine and Biology Society (EMBC)*, 2016, pp. 2222–2227.
9. L. Saccares, I. Sarakoglou, and N. G. Tsagarakis, "iT-Knee: An exoskeleton with ideal torque transmission interface for ergonomic power augmentation," in *IEEE/RSJ International Conference on Intelligent Robots and Systems (IROS)*, 2016, pp. 780–786.
10. D. Cai *et al.*, "Self-adjusting, isostatic exoskeleton for the human knee joint," in *Annual International Conference of the IEEE Engineering in Medicine and Biology Society*, 2011, pp. 612–618.
11. P. Walker, J. Rovick, and D. Robertson, "The effects of knee brace hinge design and placement on joint mechanics," *Journal of biomechanics*, vol. 21, no. 11, pp. 969–974, 1988.
12. D. Wilson *et al.*, "The components of passive knee movement are coupled to flexion angle," *Journal of Biomechanics*, vol. 33, no. 4, pp. 465–473, 2000.
13. D. A. Neumann, *Kinesiology of the musculoskeletal system: foundations for rehabilitation*. Elsevier Health Sciences, 2013.
14. E. S. Grood and W. J. Suntay, "A joint coordinate system for the clinical description of three-dimensional motions: application to the knee," *Journal of biomechanical engineering*, vol. 105, no. 2, pp. 136–144, 1983.
15. M. Lafortune *et al.*, "Three-dimensional kinematics of the human knee during walking," *Journal of Biomechanics*, vol. 25, no. 4, pp. 347–357, 1992.
16. C. L. Collins, "Kinematics of robot fingers with circular rolling contact joints," *Journal of Robotic Systems*, vol. 20, no. 6, pp. 285–296, 2003.
17. S. H. Kim *et al.*, "Force characteristics of rolling contact joint for compact structure," in *IEEE International Conference on Biomedical Robotics and Biomechatronics (BioRob)*, 2016, pp. 1207–1212.
18. J. H. Mun and D.-W. Lee, "Three-dimensional contact dynamic model of the human knee joint during walking," *KSME International Journal*, vol. 18, no. 2, pp. 211–220, 2004.
19. J. R. Montierth, R. H. Todd, and L. L. Howell, "Analysis of elliptical rolling contact joints in compression," *Journal of Mechanical Design*, vol. 133, no. 3, 2011.
20. T. G. Nelson *et al.*, "Curved-folding-inspired deployable compliant rolling-contact element (D-CORE)," *Mechanism and Machine Theory*, vol. 96, pp. 225–238, 2016.
21. J. P. Kuntz, *Rolling link mechanisms*. Delft University of Technology, 1995.
22. J. Beil, G. Perner, and T. Asfour, "Design and control of the lower limb exoskeleton KIT-EXO-1," in *IEEE International Conference on Rehabilitation Robotics (ICORR)*, 2015, pp. 119–124.